CDF note 11087

Measurements of $\sigma(V + D^*)/\sigma(V)$ in 9.7 fb^{-1} at CDF Run II

The CDF Collaboration
URL http://www-cdf.fnal.gov
(Dated: June 21, 2014)

This note presents measurements of $\sigma(W + D^*)/\sigma(W)$ and $\sigma(Z + D^*)/\sigma(Z)$ in the W/Z leptonic decay channels using full D^* reconstruction. In a sample of W and Z events skimmed from 9.7 fb^{-1} of high-p_T muon and electron data in $p\bar{p}$ collisions at the CDF ($\sqrt{s} = 1.96$ GeV), we identify charm by fully reconstructing $D^*(2010) \to D^0(\to K\pi)\pi_s$ decays at the track level. Using a binned fit of $\Delta m = m(K\pi\pi_s) - m(K\pi)$ to count reconstructed D^* candidates, we then unfold these raw counts with acceptance values derived from Monte Carlo. All measurements are found to be in agreement with Pythia Monte Carlo predictions. This note includes the first measurement of $W/Z + D^*$ production with $p_T(c) < 15$ GeV at the Tevatron.

I. INTRODUCTION

This note describes a measurement of the production ratios $\sigma(W/Z+D^*)/\sigma(W/Z)$ in $p\bar{p}$ collisions at $\sqrt{s} = 1.96$ TeV with the CDF Run II detector at the Fermilab Tevatron. The CDF detector is described in detail elsewhere [1]. Lepton tagging and missing energy ($\not\!\!E_T$) are used for W/Z identification; tracks near the W/Z decay vertex are then searched for evidence of the decay $D^*(2010) \to D^0(\to K\pi)\pi_s$. The invariant mass difference $m(K\pi\pi_s) - m(K\pi)$ between the reconstructed vertices of D^* candidates provides a sharp signal peak at 0.1455 MeV, slightly above the charged pion mass. With no other resonant particle states in the same Δm region, the background is dominantly combinatoric.

This measurement is sensitive to many aspects of heavy-flavor physics. The $p\bar{p} \to W + c$ production process is sensitive to the magnitude of the Cabibbo-Kobayashi-Maskawa matrix element V_{cs}, and also to the strange quark distribution function of the proton [2, 3]. Additionally, measurements of $W/Z + c$ and $W/Z + g(\to c\bar{c}/b\bar{b})$ events can be used to test and improve upon models of the hadronization process [4–6]. Perhaps most importantly, an understanding of $p\bar{p} \to W/Z + c$ events helps with the wider problem of identifying signal in other physics searches: Higgs, top and dark matter candidate searches often involve final states that look very $W/Z+$ heavy flavor-like.[7, 8].

Previous analyses of $p\bar{p} \to W/Z + c$ production have measured the relative cross-sections $\sigma(W/Z+c)/\sigma(W/Z+\text{jets})$ [8, 9]. Restrictions on jet acceptance, however, limit these analyses to studying only the high-momentum $p_T(jet) >$ 20 GeV charm regime. Full reconstruction of $D^*(2010) \to D^0(\to K\pi)\pi_s$ probes a much lower $p_T(c)$ regime (mean $p_T(D^*)_{tagged} = 10\text{GeV}$, mode $p_T(D^*)_{tagged} = 6\text{GeV}$). This measurement is therefore complementary to the higher-p_T jet approaches conducted by earlier, jet-based analyses.

II. DATA SAMPLE & W/Z EVENT SELECTION

This analysis is based on the full CDF Run II dataset, with an integrated luminosity of 9.7 fb^{-1}. The data are collected with an inclusive lepton trigger that requires an electron (muon) with $E_T > 18$ GeV ($p_T > 18$ GeV/c). We collectively refer to this dataset as 'high-p_T lepton events'.

A. W/Z event selection

From this inclusive high-p_T lepton dataset we select events offline. A Z candidate is required to have two oppositely-signed electrons (muons), each with $E_T > 25$ GeV ($p_T > 20$ GeV) and $|\eta_{track}| < 1.1$; the invariant mass of the lepton pair is required to fall between 66 GeV $< m(\ell^+, \ell^-) <$ 116 GeV.

A W candidate is required to have one isolated electron (muon) with $E_T > 25$ GeV ($p_T > 20$ GeV) and $|\eta| < 1.1$, and the event must further have corrected $\not\!\!E_T > 25(20)$ GeV for $W \to e\nu(\mu\nu)$. $\not\!\!E_T$ is corrected for muons, and for offline corrections to jet energies. The lepton is considered isolated if $Iso < 0.1$, where Iso is the ratio of the total transverse energy of all sources in a cone of $\Delta R = 0.4$ about the electron (muon) track (excluding the electron (muon) being considered), to the transverse energy (momentum) of the electron (muon). The transverse mass of the W, $M_T(W) = \sqrt{2.0 \cdot E_T(\ell) \cdot \not\!\!E_T \cdot (1 - \cos(\Delta\phi_{e,\overrightarrow{E_T}}))}$, must satisfy $M_T(W) > 20$ GeV for both channels (though $E_T(\ell)$ is set equal to track p_T for muons).

B. D^* selection

For all W or Z events, we begin the search for D^* by selecting all tracks within 2.0 cm of the high-p_T lepton's point of closest approach to the beamline ($|\Delta z| < 2.0$ cm). For Z decays in which both leptons have a track, we use the point of closest approach of the highest p_T lepton identified.

For each possible set of three tracks taken from our selection, we hypothesize that one is the K, one the π, and one the π_s of a $D^*(2010) \to D^0(\to K\pi)\pi_s$ decay. This includes assigning the appropriate K or π mass to each track (*e.g.*, when calculating invariant masses). We then make a number of checks against this hypothesis in order to eliminate background.

We first require that the K and π have opposite electric charge, as determined by the curvature of their tracks in the magnetic field. Then, as $D^0 \to K^-\pi^+$ is Cabbibo-favored versus $D^0 \to K^+\pi^-$ by a factor of 10^4, we require the two pions to have the same charge. We apply a track quality cut, and further require that each track satisfy $|\eta| < 1.1$. Based on Monte Carlo (MC) simulations, we enforce lower limits $p_T(K, \pi) > 400$ MeV, $p_T(\pi_s) > 80$ MeV, and $\Delta R < 1.1$ for each pair of tracks, where$\Delta R \equiv \sqrt{\Delta\phi^2 + \Delta\eta^2}$.

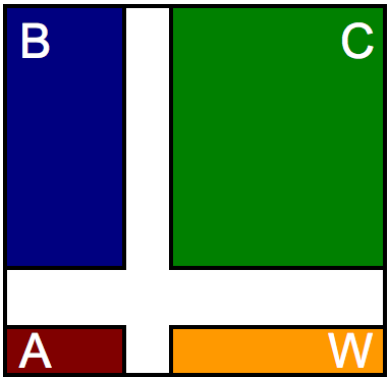

FIG. 1: Cartoon illustrating the division of the $\not\!\!E_T/Iso$ plane into four regions A, B, C, and W. Region W contains all W candidates pasing our cuts, as defined in Section III A. Regions A, B, and C, contain mostly QCD events faking the W signature. The number of QCD events observed in quadrants A, B, and C are used to estimate the number of QCD events in quadrant W, following Eq. 1 .

With these preliminary cuts in place, we use a fitting algorithm to reconstruct D^0 and D^* vertices from the K, π and π_s track candidates. Because we are interested not only in direct charm, but also in charm from bottom decays (Wbb events), we do not require the D^* to point back towards the beamline. We reject events only if the fit probability is 0 (e.g. the fit did not converge). These non-zero fit probabilities are used later to eliminate background. Finally, we require the fitted D^0 mass to fall within $3\sigma = 0.03321$ GeV of the nominal D^0 mass peak, $m_{D^0} = 1.865$ GeV.

III. BACKGROUNDS

A. Estimating W/Z backgrounds

Background in Z events is estimated only in the context of Section IV A. Background in W events is determined by relaxing cuts on lepton isolation Iso and missing energy $\not\!\!E_T$, and defining four regions A, B, C, and W in the $\not\!\!E_T/Iso$ plane; region W is our signal region as defined earlier, and the rest are are chosen to have $\not\!\!E_T$ and Iso incompatible with most real W events (see Figure 1). To first order, events in regions A, B, and C are QCD events faking the W signature. We estimate

$$N^W_{QCD} = \frac{N^W_{QCD}}{N^B_{QCD}} \times N^C_{QCD} \tag{1}$$

where N^X_{QCD} is the number of QCD events in region X. To get N^X_{QCD}, we must estimate the number of EWK events in each region. Using MC predictions scaled to an (unknown) count of $W \to \mu\nu/e\nu$ signal events in signal region W, we estimate the number of EWK events ($Z \to \ell^+\ell^-$, $W \to \ell\nu$) in each quadrant. These predicted EWK counts are subtracted from the total event counts in each region, in order to determine the number of QCD events that remain. By leaving the final count of real W events in signal region W unknown, we end up with an equation for the number of real $W \to \mu\nu/e\nu$ signal events in region W. Explicitly, we write

$$N^X_{QCD} = N^X_{total} - \left(R^X_{W\to\mu\nu} + R^X_{W\to\tau\nu} + R^X_{Z\to\mu\mu}\right) N^X_{W\to\mu\nu/e\nu} \tag{2}$$

where N^X_{toal} is the count of all events in region X, and $R^X_{Y\to fg}$ is the fraction of events in region X which are predicted to be of type $Y \to fg$, over the unknown count of real signal events in region W ($N^W_{W\to\mu\nu/e\nu}$). Putting eq. 2 into eq. 1, we solve for the number of $W \to \mu\nu/e\nu$ signal events in region W; we then work backwards to count the number of EWK, QCD and signal events in each region of the $\not\!\!E_T/Iso$ plane.

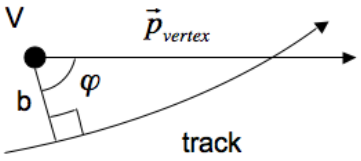

FIG. 2: Sketch of a track and vertex for which b_s might be calculated. ϕ is the angle between the momentum of the reconstructed vertex, and the line connecting the track and vertex at the point of closest approach. b is the distance between the track and vertex at this point.

	Variable		Variable
1	$L_{xy}(D^0)$	11	$L_{xy}(D^*)$
2	$p_T(K)$	12	$p_T(D^*)$
3	$b_s(\pi_s, D^*)$	13	$p_T(\pi_s)$
4	$\Delta R(K, \pi)$	14	$\Delta R(K, \pi_s)$
5	$b_s(\pi, D^*)$	15	$b_s(D^0,$ beam$)$
6	$b_s(K, D^0)$	16	$\lvert\mathbf{V}_{D^*} - \mathbf{V}_{D^0}\rvert$
7	$\Delta R(\pi, \pi_s)$	17	Vtx Lxy
8	Fit χ^2/DOF	18	$b_s(K, D^*)$
9	$p_T(\pi)$	19	$b_s(\pi, D^0)$
10	$b_s(D^*,$ beam$)$		

TABLE I: The properties used to characterize our D^* candidates, both signal and background. It is these properties that the neural networks uses to separate signal and background.

B. Reducing D^* background with a neural network

To reduce the number of background events which pass the D^* selection cuts (Section II B), we train a neural network to discriminate among D^* candidates using 19 descriptive variables (see Table I). We include custom variables b_s, which describe the point of closest approach between a track and the D^* or D^0 vertex. b_s is defined as $b_s(\text{track}, \text{Vtx}) \equiv b \cdot \text{sign}(\cos(\phi))$, with ϕ as defined in Fig 2. These parameters are complementary to the L_{xy} measurements, and provide a more detailed look into the kinematics of our decay. We also define $b_s(D^*/D^0, \text{beam})$, using the reconstructed D^*/D^0 momenta to find b and ϕ of the D^*/D^0 particles' path with respect to the beamline.

To train our neural network, we use a Monte Carlo signal sample of $W + D^*$ events, simulated using the cdfSim package. After reconstructing all D^* candidates in these events according to the process described in Section II B, we define all candidates that fall within $3\sigma = 0.00288$ of the Δm peak, $\Delta m_{peak} = 0.1455$ as Monte Carlo signal.

To model background, we choose D^* candidates in data which pass all of our cuts in Section II B, but whose tracks do not have the proper sign relations. There are two such backgrounds: "same-sign track" (SS) background, in which all tracks have the same sign; and "bad-sign π_s" (BPS) background, in which the soft pion has the opposite charge of the pion from $D^0 \to K\pi$. The SS background is dominantly combinatoric; the BSP background combines combinatoric background, real $D^0 \to K^+\pi^-$ decays paired with a random low-momentum track, and signal events with misreconstructed soft pion signs. Influence from this latter category of events is automatically folded into our acceptance times efficiency calculations (see Section VI). To keep background events as signal-like as possible, we require these background D^* candidates to fall within 3.2σ of the peak (a compromise that allows an equal number of signal and background events for neural network training).

With neural network scores confined to the region $NN_{score} = [-1.0, 1.0]$, we require D^* candidates in data to satisfy $NN_{score} > 0.0$. This eliminates $\sim 80\%$ of background and $\sim 10\%$ of signal. We bin $\Delta m \equiv m(K\pi\pi_s) - m(K\pi)$ for all candidates which pass the neural network cut, and fit the Δm distribution to a power-law background plus double-gaussian signal We use a template for the double-gaussian; the template is taken from a fit to simulated Monte Carlo signal events; before applying the template to fits in data, its width is enhanced by a factor of 1.1 to account for lower resolution in data).

From the $W \to e\nu$ and $W \to \mu\nu$ samples, we count $N_{W(e\nu)+D^*} = 340 \pm 30$ and $N_{W(\mu\nu)+D^*} = 294 \pm 26$. Combining results from the muon and electron samples, we count $N_{W(\mu\nu/e\nu)+D^*} = 634 \pm 39$, and $N_{Z(\mu\mu/ee)+D^*} = 42 \pm 11$ (Figure 3).

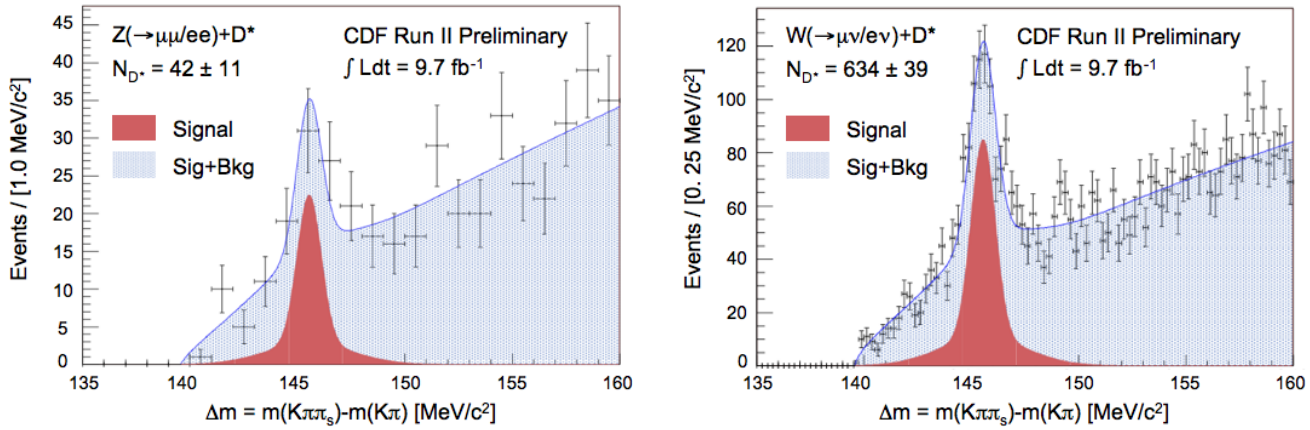

FIG. 3: Fitted plots of D^* signal discriminant Δm for D^* candidates in both W and Z events. The electron and muon decay modes are combined. In order for an event to be tagged, the charged lepton(s) from the $W(Z)$ decay and all final products of the D^* decay must satisfy $|\eta| < 1.1$.

IV. DETERMINING FRACTIONS $f_{D^*}^{W/Z} \equiv N_{W/Z+D^*}/N_{W/Z}$

The counts $N_{W(\mu\nu/e\nu)+D^*}$ and $N_{Z(\mu\mu/ee)+D^*}$ as reported in the previous section contain D^* from W/Z events, and D^* from W/Z background events (*e.g.*, a QCD event faking the W signature, but produced in association with a real D^*). We must account for this in order to report ratios $\sigma(W/Z + D^*)/\sigma(W/Z)$.

A. Finding the $Z + D^*$ rate

We define two regions along the invariant mass axis, $m_Z(\ell^+\ell^-)$, for all Z candidates: the signal region is defined as $|m_Z - 91 \text{ GeV}| \leq 3\sigma$, and the background region is defined as $|m_Z - 91 \text{ GeV}| > 3\sigma$ ($\sigma = 2.0$ (3.0) for $Z \to \mu\mu$ ($Z \to ee$), We fit the m_Z distribution to a double-gaussian signal plus exponential background hypothesis, and integrate beneath the curves to count signal and background events in each region, $N_Z^{\text{sig/bkg region}}$ and $N_{Bkg}^{\text{sig/bkg region}}$. For each region, we then bin Δm for all D^* candidates, and fit the resulting distribution with our previously-described Δm signal plus background hypothesis. This gives us counts $N_{D^*}^{\text{sig region}}$ and $N_{D^*}^{\text{bkg region}}$. Now, we can construct two simple coupled equations to solve for the rate of background plus D^* events, $f_{D^*}^{Z,bkg}$, and signal plus D^* events, $f_{D^*}^{Z,sig}$. (Equation 3).

$$\begin{aligned} N_{D^*}^{\text{Z, sig region}} &= f_{D^*}^{\text{Z,sig}} \cdot N_Z^{\text{sig region}} + f_{D^*}^{bkg} \cdot N_{Bkg}^{\text{Z, sig region}} \\ N_{D^*}^{\text{Z, bkg region}} &= f_{D^*}^{\text{Z,sig}} \cdot N_Z^{\text{bkg region}} + f_{D^*}^{bkg} \cdot N_{Bkg}^{\text{Z, bkg region}} \end{aligned} \tag{3}$$

B. Finding the $W + D^*$ rate

We have three non-signal sources of D^* in our W signal region: $W \to \tau\nu$, $Z \to \ell\ell$, and QCD events.

We first assume that our measured rates $f_{D^*}^{Z,sig}$ for each Z decay mode, as described in the previous subsection, should be equal across all $\not\!\!E_T/Iso$ regions as defined in Figure 1. We also assume that the (unknown) rate of $W + D^*$ production, $f_{D^*}^{W,sig}$, should be approximately equal for $W \to \tau\nu$ 'background' and $W \to \mu\nu/e\nu$ signal events, and that it too should be approximately equal across all $\not\!\!E_T/Iso$ regions.

This leaves the question of D^* production in QCD-background-faking-W events. There is no *a priori* reason to assume that the rate at which QCD events are produced in association with D^*, $f_{D^*}^{\text{QCD}}$, is constant across all four quadrants. We therefore explicitly measure the dependence of $f_{D^*}^{\text{QCD}}$ on $\not\!\!E_T$ and Iso. To do so, we assume that $f_{D^*}^{\text{QCD}}$ can be written as

$$f_{D^*}^{\text{QCD}} = h(MET) \times g(Iso)$$

To first order, then, we write

$$f^{\rm QCD}_{D^*,A} = h_{LO} \times g_{LO} \qquad f^{\rm QCD}_{D^*,B} = h_{LO} \times g_{HI} \qquad f^{\rm QCD}_{D^*,C} = h_{HI} \times g_{HI}$$

where $f^{\rm QCD}_{D^*,X}$ is defined as the rate of *QCD* background plus D^* production in Region X. We can then write

$$f^{\rm QCD}_{D^*,W} = h_{HI} \times g_{LO} = \frac{f^{\rm QCD}_{D^*,A} \times f^{\rm QCD}_{D^*,C}}{f^{\rm QCD}_{D^*,B}} \tag{4}$$

Note that by counting the number of D^* in each quadrant, we have four values which can be used to solve for four unknown rates. Using $f^{Z\to\mu\mu/ee}_{D^*}$ rates measured according to the previous section, we choose these four unknown rates to be $f^{\rm QCD}_{D^*,A}$, $f^{\rm QCD}_{D^*,B}$, $f^{\rm QCD}_{D^*,C}$, and $f^{\rm W}_{D^*}$. We solve for these unknowns in an iterative process: assume that we have some estimate for $f^{W}_{D^*}$; subtract from each region the number of D^* expected to be from all EWK sources; divide the remaining D^* count by the number of *QCD* events in quadrants, A, B, and C, to find $f^{\rm QCD}_{D^*,A}$, $f^{\rm QCD}_{D^*,B}$, and $f^{\rm QCD}_{D^*,C}$; calculate $f^{\rm QCD}_{D^*,W}$ using Eq 4; using $f^{\rm QCD}_{D^*,W}$ and $f^{Z}_{D^*}$, subtract out non-W sources of D^* in region W; and finally, divide the remaining number of D^* in that region by the number of W in that region to get a next-order approximation to $f^{W}_{D^*}$.

With an initial guess of $f^{W}_{D^*} = 0$, we iterate through this process until the value of $f^{W}_{D^*}$ does not change by more than 0.1% of its value over two consecutive iterations. (This is far lower than the uncertainty in our Δm signal fits, see Figure 3—as such, there is no need to iterate further.)

V. SPLITTING THE $W + D^*$ SAMPLE BY PRODUCTION PROCESS

As explained in the introduction, $W + D^*$ events are expected to come from three different production processes. We recall the relevant production processes (and define the abbreviations with which we will refer to them) here:

$$\begin{aligned} q + \bar{q}' \to W + g(\to c\bar{c}) \to W + D^* + X \;&\equiv\; Wcc \\ q + g \to W + c \to W + D^* + X \;&\equiv\; Wc \\ q + \bar{q}' \to W + g(\to b\bar{b}) \to W + D^* + X \;&\equiv\; Wbb \end{aligned} \tag{5}$$

In this section, we determine what fraction of our $W + D^*$ signal sample comes from each one of these production processes. We write these production process fractions as X^Y, where Y is one of the three production processes listed above, $Y \in [Wcc, Wbb, Wc]$, and X is the fraction of all tagged D^* in the signal that come from Y.

A. Using neural networks to find the fraction of Wbb events

Due primarily to a difference in $p_T(D^*)$ spectra, a neural network will generally identify D^* from different sources (*Wcc*, *Wc*, and *Wbb*) with different efficiencies. We can take advantage of this to measure the fraction of our signal that comes from each of these three production processes.

We first train three neural networks, using the same variables described in Table I: NN_{Wcc}, NN_{Wc}, and NN_{Wbb}. Each network is trained to identify one type of signal event (labeled in the subscript) versus the *BSP* and *SS* background samples described in Section III B. We run each of these three neural networks over each of our three signal sample (*Wcc*, *Wc,* and *Wbb*), and collect the scores given by each neural network to each D^* candidate.

Next, we run our pre-neural network $W + D^*$ selection (candidates as found in Section II B) through each neural network, recording the score that each network gives to each event. We then add a second layer of three new neural networks: $NN_{Wcc\ \mathrm{vs}\ Wbb}$, $NN_{Wbb\ \mathrm{vs}\ Wcc}$, and $NN_{Wc\ \mathrm{vs}\ Wcc}$. As the subscripts would imply, each new neural network is trained to identify one type of production process as signal, and another as 'background'. This provides further separation between the three types of production process, which in turn allows finer measurement of production process fractions X^Y. We train these new neural networks not only on the standard set of D^* properties (Table I), but also on the score that each event is given by the original three neural networks NN_{Wcc}, NN_{Wc}, and NN_{Wbb}.

Grouping each first-order neural network with one second order neural network (specifically NN_{Wcc}+$NN_{Wcc\ \mathrm{vs}\ Wbb}$, $NN_{Wbb} + NN_{Wbb\ \mathrm{vs}\ Wcc}$, and $NN_{Wc} + NN_{Wc\ \mathrm{vs}\ Wcc}$), and requiring that a D^* candidate have a score > 0 for both

neural networks in a given set, we find three new efficiencies. We then run our pre-neural network $W + D^*$ selection (candidates as found in Section II B) through each set of neural networks, to obtain three new counts N_{D^*}. Putting these new efficiencies and N_{D^*} counts into equation 6, we solve to find fractions X^{Wc}, X^{Wcc}, and X^{Wbb}.

$$\begin{pmatrix} \epsilon(NN_{Wcc})_{Wcc}, & \epsilon(NN_{Wcc})_{Wc}, & \epsilon(NN_{Wcc})_{Wbb}, \\ \epsilon(NN_{Wc})_{Wcc}, & \epsilon(NN_{Wc})_{Wc}, & \epsilon(NN_{Wc})_{Wbb}, \\ \epsilon(NN_{Wbb})_{Wcc}, & \epsilon(NN_{Wbb})_{Wc}, & \epsilon(NN_{Wbb})_{Wbb}, \end{pmatrix} \begin{pmatrix} X^{Wcc} \cdot N_{D^*}^{TOT} \\ X^{Wc} \cdot N_{D^*}^{TOT} \\ X^{Wbb} \cdot N_{D^*}^{TOT} \end{pmatrix} = \begin{pmatrix} N_{D^*}^{NN_{Wcc}} \\ N_{D^*}^{NN_{Wc}} \\ N_{D^*}^{NN_{Wbb}} \end{pmatrix} \tag{6}$$

This method gives good resolution for X^{Wbb}, but is not very effective at determining the fraction X^{Wc}, due to similarities between D^* from Wcc and D^* from Wc. The next section discusses a method for more precise measurement of X^{Wc}.

B. Using W and D^* signs to find the fraction of Wc events

In the case of Wc production ($q + g \to W + c \to W + D^* + X$), conservation of charge requires that the W and c be produced with opposite signs. When the W decays leptonically, the lepton will always have the same sign as the W. When the c hadronizes to a D^*, the c and D^* will have the same sign as one-another. In sum, this means that for a Wc event, the W and D^* that we tag ought to have opposite signs. We refer to such events as $(W + D^*)_{OS}$.

In the case of either Wcc or Wbb production, however, the W is produced along with a c and $\bar{c}$ (or b and $\bar{b}$), either of which could give rise to the D^* that we tag. This means that in a Wcc or Wbb event, we are equally likely to tag oppositely-signed W and D^*, $(W + D^*)_{OS}$, or same-signed W and D^*, $(W + D^*)_{SS}$.

By considering the difference between the number of $(W + D^*)_{OS}$ and $(W + D^*)_{SS}$ events tagged by our algorithm, we can estimate the contributions of Wc events versus Wcc/Wbb events. Quantitatively,

$$N_{OS} = N_{Wc} + \frac{1}{2} N_{Wcc/Wbb}$$

$$N_{SS} = \frac{1}{2} N_{Wcc/Wbb}$$

and so

$$N_{Wc} = N_{OS} - N_{SS}$$

such that

$$X^{Wc} = \frac{N_{OS} - N_{SS}}{N_{OS} + N_{SS}}$$

VI. ACCEPTANCE RATES

We cannot assume *a priori* that our total (geometric plus kinematic plus neural network) acceptance $A \cdot \epsilon$ for inclusive W/Z events is equal to our acceptance for W/Z produced in association with D^*. These acceptances may not cancel out, therefore, in the quantity $\sigma(W/Z + D^*)\sigma(W/Z)$. We must find two acceptance rates for each of our samples: the acceptance for inclusive W/Z, and the total acceptance for $W/Z + D^*$ events (both the W/Z and the D^* are tagged).

To determine the W/Z acceptances, we run our W/Z tagging algorithms over inclusive Monte Carlo samples (one for each of the four modes considered: $W \to \mu\nu$, $W \to e\nu$, $Z \to \mu\mu$, and $Z \to ee$). To determine the $W/Z + D^*$ acceptances, we run our combined $W/Z + D^*$ tagging algorithms over simulated $W/Z + D^*$ samples (again, one for each of the four vector boson modes). All Monte Carlo samples are generated using Pythia 6.2 and simulated with cdfSim. For $W/Z + D^*$, we find acceptance both for the inclusive set of all events with $p_T(D^*) > 3$ GeV, and differentially as a function of $p_T(D^*)$. In this differential case, bins are chosen such that the expected number of tagged D^* in each bin is approximately constant, according to Monte Carlo simulations. The lowest bin boundary at $p_T(D^*) = 3$ GeV is chosen due to vanishing $A \cdot \epsilon$ for $p_T(D^*) < 3$ GeV.

As an example, we show $A \cdot \epsilon$ as a function of $p_T(D^*)$ for simulated $W(\to \mu\nu) + D^*$ events in Figure 4. The inclusive rates for W/Z selection, and for $p_T(D^*) > 3$ GeV, are shown in Table II.

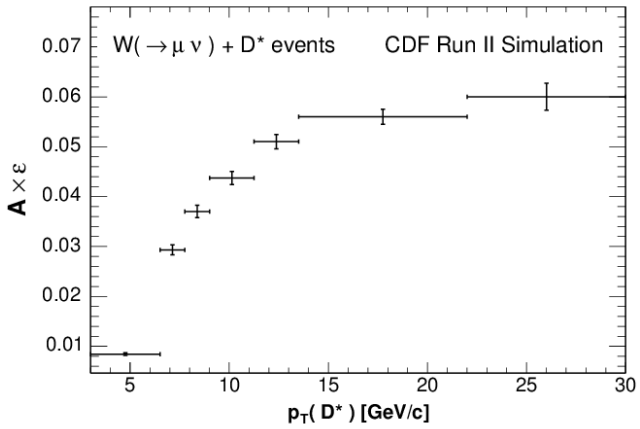

FIG. 4: Plot of $A \cdot \epsilon$ as a function of $p_T(D^*)$ for simulated $W(\rightarrow \mu\nu) + D^*$ events. The x-axis has been split into bins chosen such that the expected number of D^* tagged in each bin region is approximately constant according to Monte Carlo simulation. Monte Carlo events are generated using Pythia 6.2 and simulated using cdfSim. The displayed bin-wise limits on $p_T(D^*)$ are the only kinematic restriction on these acceptance values.

CDF Run II Simulation

Process (with D^* understood to decay as $D^* \rightarrow D^0(\rightarrow K\pi)\pi$)	Inclusive W/Z tag rate ($(A \cdot \epsilon)_W$) ($\times 10^{-2}$)	Inclusive $W/Z + D^*$ tag rate w/ NN ($(A \cdot \epsilon)_{W+D^*}$) ($p_T(D^*) > 3$ GeV/c)($\times 10^{-2}$)
$p\bar{p} \rightarrow W(\rightarrow e\nu) + D^*$	19.5 ± 0.2	2.13 ± 0.03
$p\bar{p} \rightarrow W(\rightarrow \mu\nu) + D^*$	21.9 ± 0.3	2.42 ± 0.04
$p\bar{p} \rightarrow Z(\rightarrow ee) + D^*$	4.8 ± 0.1	0.94 ± 0.03
$p\bar{p} \rightarrow Z(\rightarrow \mu\mu) + D^*$	6.1 ± 0.1	1.24 ± 0.03

TABLE II: Rates of geometric plus kinematic acceptance for inclusive W/Z events, and for $W/Z + D^*$ events after applying a neural network cut to reduce background. Rates are found by running over events generated using Pythia 6.2 and simulated using cdfSim. We look at the muon and electron modes separately, for each the W and Z cases. Uncertainty is dominated by uncertainty in the proton parton distribution function (PDF). The displayed restriction on $p_T(D^*)$ is the only kinematic restriction on these acceptance values.

VII. SYSTEMATIC UNCERTAINTIES

A. Systematic uncertainty in $Z + D^*$ rates

To estimate the systematic uncertainty of this method, we perform the above analysis for several definitions of the signal and background region. We fit the set of all $f_{D^*}^{Z,sig}$ values found using these definitions to a constant value hypothesis, and take the uncertainty in this fit to be our systematic uncertainty. This is done separately for each of our Z samples, $Z \rightarrow \mu\mu$ and $Z \rightarrow ee$. We find a systematic uncertainty of 20% for the $Z(\rightarrow \mu\mu) + D^*$ measurement, and a systematic uncertainty of 11% for the $Z(\rightarrow ee) + D^*$ measurement.

B. Systematic uncertainty in $W + D^*$ rates

To estimate the systematic uncertainty of this method, we perform this analysis for several definitions of the regions A, B, C and W as defined in Figure 1, first keeping the Iso boundaries fixed and varying the $\not\!\!E_T$ boundaries, and then keeping the $\not\!\!E_T$ boundaries fixed and varying the Iso boundaries. This is done separately for each of our W samples, $W \rightarrow \mu\nu$ and $W \rightarrow e\nu$. We find a systematic uncertainty of 10% in the $W(\rightarrow e\nu) + D^*$ measurement, and a

systematic uncertainty of 2% in the $W(\to \mu\nu) + D^*$ measurement.

C. Systematic uncertainty in signal modeling / proton PDF

The only remaining non-negligible source of systematic uncertainty in our results is that in our measurements of $A \cdot \epsilon$. Some of this statistical, and due to the finite size of our simulated $W/Z + D^*$ event samples (signal modeling uncertainty). The rest is due to uncertainty in the proton parton distribution function CTEQ (PDF uncertainty). PDF acceptance uncertainties are set using the 40 CTEQ eigenvectors with 90% confidence level (CL) variations. The MSTW2008 central value is checked versus the CTEQ central value. If the difference between CTEQ and MSTW2008 is smaller than the uncertainty from the 40 eigenvectors, no additional uncertainty is taken. If the difference is larger, that difference is taken as an additional systematic added in quadrature to the eigenvector uncertainty. Uncertainty in $\alpha_s(M_Z)$ ($\pm$90% CL) is taken as an additional systematic, and added in quadrature to the above.

D. Total uncertainties

We collect all statistical and systematic uncertainties together with our final results in Table III. All uncertainties that are not listed in this table are considered to be negligible. Common sources of uncertainty in measurements of total cross-section (*e.g.* luminosity and trigger efficiency uncertainties), cancel to within a negligible amount when taking the ratio $\sigma(V + D^*)/\sigma(V)$.

VIII. FINAL RESULTS

A. Final measurements of $\sigma(W/Z + D^*)/\sigma(W/Z)$

Using the branching ratio for $D^* \to D^0(\to K\pi)\pi_s$, $\mathrm{Br}_{D^*\to D^0(\to K\pi)\pi_s} = 0.0263 \pm 0.0004$ [10], we unfold raw fractions $f_{D^*}^{W/Z}$ to ratios $\sigma(W/Z + D^*)/\sigma(W/Z)$ as

$$\frac{\sigma\big(W/Z + D^*\big)}{\sigma\big(W/Z\big)} = f_{D^*}^{W/Z} \cdot \frac{A \cdot \epsilon_W}{A \cdot \epsilon_{W+D^*} \times \mathrm{Br}_{D^*\to D^0(\to K\pi)\pi_s}} \tag{7}$$

We first unfold $f_{D^*}^{W/Z}$ for the inclusive set of events $p_T(D^*) > 3$ GeV; for the W samples only, we then unfold $f_{D^*}^{W}$ differentially as a function of $p_T(D^*)$. Results from the electron and muon decay channels are then combined using a best linear uncertainty estimate (BLUE), assuming that for each the W and Z samples, systematic uncertainties are fully correlated across decay modes. Results are shown in Tables IV and V, and Figures 5, 6.

B. Final measurements of production process fractions

Recall that $W + D^*$ events are expected to come from three different production processes. We recall the relevant production processes (and the abbreviations with which we will refer to them) here:

$$\begin{aligned} q + \bar{q}' \to W + g(\to c\bar{c}) \to W + D^* + X &\equiv Wcc \\ q + g \to W + c \to W + D^* + X &\equiv Wc \\ q + \bar{q}' \to W + g(\to b\bar{b}) \to W + D^* + X &\equiv Wbb \end{aligned} \tag{8}$$

Our only measurement of the fraction of the D^* signal that comes from Wbb production, comes from the process described in Section V A; our most precise measurement of the fraction of the D^* signal that comes from Wc production, comes from the process described in Section V B. Because a different technique was used to find each fraction, we treat the uncertainties in each measurement as uncorrelated. Assuming that the remaining fraction of all $W + D^*$ events tagged comes from the Wcc process, we report final fractions in Table VI.

Inclusive sample $\int \mathcal{L}dt = 9.7$ fb^{-1} $p_T(D^*) > 3.0$ GeV/c	CDF Run II Preliminary $\frac{\sigma(V+D^*)}{\sigma(V)}$ $(\times 10^{-2})$	% **stat unc.**	Bkgs. % syst unc.	Signal modeling % syst unc.	PDF % syst unc.	**Total % syst unc.**
$W(\to e\nu) + D^*$	1.74	**12**	10	$\ll 1$	2	**10**
$W(\to \mu\nu) + D^*$	1.75	**10**	2	$\ll 1$	2	**3**
$Z(\to ee) + D^*$	1.0	**57**	19	$\ll 1$	1	**19**
$Z(\to \mu\mu) + D^*$	1.8	**30**	11	$\ll 1$	1	**11**

$W(\to e\nu) + D^*$ $\int \mathcal{L}dt = 9.7$ fb^{-1} $[p_T(D^*)$ range$]$ (GeV/c)	CDF Run II Preliminary $\frac{d\sigma(V+D^*)}{\sigma(V)\cdot dp_T(D^*)}$ [GeV/c]$^{-1}(\times 10^{-3})$	% **stat unc.**	Bkgs. % syst unc.	Signal modeling % syst unc.	PDF % syst unc.	**Total % syst unc.**
$[3.0, 6.50]$	2.77	**29**	6	3	2	**7**
$[6.50, 7.75]$	1.60	**29**	6	3	2	**7**
$[7.75, 9.00]$	0.73	**45**	12	3	2	**13**
$[9.00, 11.25]$	0.44	**37**	15	3	3	**15**
$[11.25, 13.5]$	0.40	**36**	11	2	3	**12**
$[13.5, 21.75]$	0.21	**22**	15	4	3	**16**
$[21.75, 30.00]$	0.10	**21**	7	4	4	**9**

$W(\to \mu\nu) + D^*$ $\int \mathcal{L}dt = 9.7$ fb^{-1} $[p_T(D^*)$ range$]$ (GeV/c)	CDF Run II Preliminary $\frac{d\sigma(V+D^*)}{\sigma(V)\cdot dp_T(D^*)}$ [GeV/c]$^{-1}(\times 10^{-3})$	% **stat unc.**	Bkgs. % syst unc.	Signal modeling % syst unc.	PDF % syst unc.	**Total % syst unc.**
$[3.0, 6.50]$	3.69	**21**	5	2	2	**6**
$[6.50, 7.75]$	1.44	**31**	16	3	2	**16**
$[7.75, 9.00]$	1.21	**27**	3	3	2	**4**
$[9.00, 11.25]$	0.64	**25**	4	2	2	**5**
$[11.25, 13.5]$	0.29	**38**	3	2	2	**4**
$[13.5, 21.75]$	0.17	**21**	4	2	2	**5**
$[21.75, 30.00]$	0.08	**28**	4	3	3	**6**

TABLE III: A summary of statistical and systematic uncertainties in our final results. Our statistical uncertainty is dominated by uncertainty from our fits of the Δm signal plus background plots, while our systematic uncertainty is dominated by the methods used to find our tagged fractions, labeled above as "Bkgs." Uncertainty due to finite sample size in our evaluation of $A \cdot \epsilon$ is identified as "signal modeling", while PDF uncertainties in $A \cdot \epsilon$ are labeled as such. Uncertainties not mentioned here are considered negligible. Many uncertainties (e.g., luminosity and trigger uncertainties) are almost entirely cancelled out by taking the ratio of cross-sections; this is one of the advantages to measuring this ratio, versus a total cross-section.

Production process $(p_T(D^*) > 3$ GeV/c)	CDF Run II Preliminary $\int \mathcal{L}dt = 9.7$ fb^{-1} $\sigma(V+D^*)/\sigma(V)$ (%) $\pm$(stat) $\pm$ (syst)	Pythia 6.2.16 (CTEQ5L) $\sigma(V+D^*)/\sigma(V)$ (%) $\pm$ (pdf unc)
$W(\to e\nu) + D^*$	$1.74 \pm 0.21 \pm 0.17$	1.77 ± 0.07
$W(\to \mu\nu) + D^*$	$1.75 \pm 0.17 \pm 0.05$	1.77 ± 0.07
Combined results: $W(\to e\nu/\mu\nu) + D^*$	$1.75 \pm 0.13 \pm 0.09$	1.77 ± 0.07
$Z(\to ee) + D^*$	$1.0 \pm 0.6 \pm 0.2$	1.36 ± 0.05
$Z(\to \mu\mu) + D^*$	$1.8 \pm 0.5 \pm 0.2$	1.36 ± 0.05
Combined results: $Z(\to ee/\mu\mu) + D^*$	$1.5 \pm 0.4 \pm 0.2$	1.36 ± 0.05

TABLE IV: The ratio of cross-sections $\sigma(W/Z + D^*)/\sigma(W/Z)$ for inclusive sample $p_T(D^*) > 3$ GeV, and the predictions of Pythia 6.2.16 simulation using PDF set CTEQ5L. The displayed restriction on $p_T(D^*)$ is the only kinematic restriction on these unfolded results. The results from each decay mode are combined using a best linear uncertainty estimate, with systematic uncertainties assumed to be fully correlated. These are the final values, with full statistical and systematic uncertainties.

$p_T(D^*)$ Range [GeV/c]	CDF Run II Preliminary $\int \mathcal{L}dt = 9.7$ fb^{-1} Data			Pythia 6.2.16 (CTEQ5L)
	$\frac{d\sigma(W_{e\nu}+D^*)}{\sigma(W_{e\nu})\cdot dp_T(D^*)}$	$\frac{d\sigma(W_{\mu\nu}+D^*)}{\sigma(W_{\mu\nu})\cdot dp_T(D^*)}$	$\frac{d\sigma(W_{e\nu/\mu\nu}+D^*)}{\sigma(W_{e\nu/\mu\nu})\cdot dp_T(D^*)}$	$\frac{d\sigma(W_{e\nu/\mu\nu}+D^*)}{\sigma(W_{e\nu/\mu\nu})\cdot dp_T(D^*)}$
	[GeV/c]$^{-1}$ $\times 10^{-3}$ $\pm$(stat) $\pm$ (syst)	[GeV/c]$^{-1}$ $\times 10^{-3}$ $\pm$(stat) $\pm$ (syst)	[GeV/c]$^{-1}$ $\times 10^{-3}$ $\pm$(stat) $\pm$ (syst)	[GeV/c]$^{-1}$ $\times 10^{-3}$ $\pm$(stat) $\pm$ (syst)
$[3.0, 6.50]$	$2.8 \pm 0.9 \pm 0.2$	$3.7 \pm 0.8 \pm 0.2$	$3.3 \pm 0.6 \pm 0.2$	2.44 ± 0.07
$[6.50, 7.75]$	$1.60 \pm 0.48 \pm 0.08$	$1.44 \pm 0.48 \pm 0.24$	$1.53 \pm 0.34 \pm 0.15$	2.01 ± 0.09
$[7.75, 9.00]$	$0.73 \pm 0.32 \pm 0.08$	$1.21 \pm 0.32 \pm 0.07$	$0.97 \pm 0.23 \pm 0.08$	0.99 ± 0.04
$[9.00, 11.25]$	$0.44 \pm 0.18 \pm 0.09$	$0.64 \pm 0.16 \pm 0.04$	$0.56 \pm 0.12 \pm 0.06$	0.73 ± 0.04
$[11.25, 13.5]$	$0.40 \pm 0.13 \pm 0.09$	$0.29 \pm 0.11 \pm 0.02$	$0.32 \pm 0.09 \pm 0.04$	0.47 ± 0.04
$[13.5, 22.0]$	$0.21 \pm 0.05 \pm 0.02$	$0.17 \pm 0.04 \pm 0.01$	$0.17 \pm 0.03 \pm 0.01$	0.20 ± 0.02
$[22.0, 30.0]$	$0.13 \pm 0.03 \pm 0.01$	$0.083 \pm 0.024 \pm 0.007$	$0.102 \pm 0.018 \pm 0.008$	0.12 ± 0.01

TABLE V: The ratio of cross-sections $\sigma(W + D^*)/\sigma(W)$ found in data as a function of $p_T(D^*)$, and the predictions of Pythia 6.2.16 using PDF set CTEQ5L. The displayed restrictions on $p_T(D^*)$ are the only kinematic restriction on these unfolded results. The results from each decay mode are combined using a best linear uncertainty estimate, with systematic uncertainties assumed to be fully correlated. These are the final results, with full statistical and systematic uncertainties.

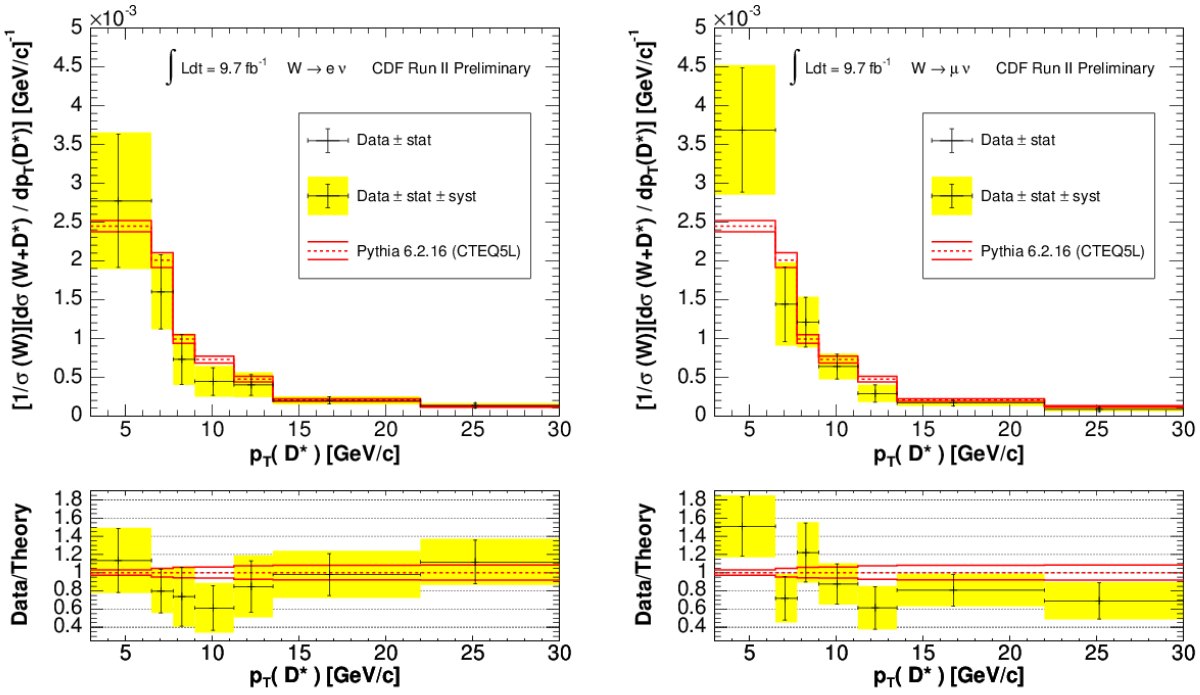

FIG. 5: The ratio of physical cross-sections $\sigma(W + D^*)/\sigma(W)$ as a function of $p_T(D^*)$. The left plot is for the $W \to e\nu$ decay mode; the right is for the $W \to \mu\nu$ decay mode. The displayed restrictions on $p_T(D^*)$ are the only kinematic restriction on these results. In each case, error bars give the statistical uncertainty, while the sum in quadrature of the statistical and systematic errors is shown as a yellow error band. The dotted red line shows the prediction of the Pythia 6.2 obtained using the CTEQ5L PDF set, with solid red lines showing PDF uncertainty in this prediction. The ratio of the simulated distribution to data is shown in the lower panels.

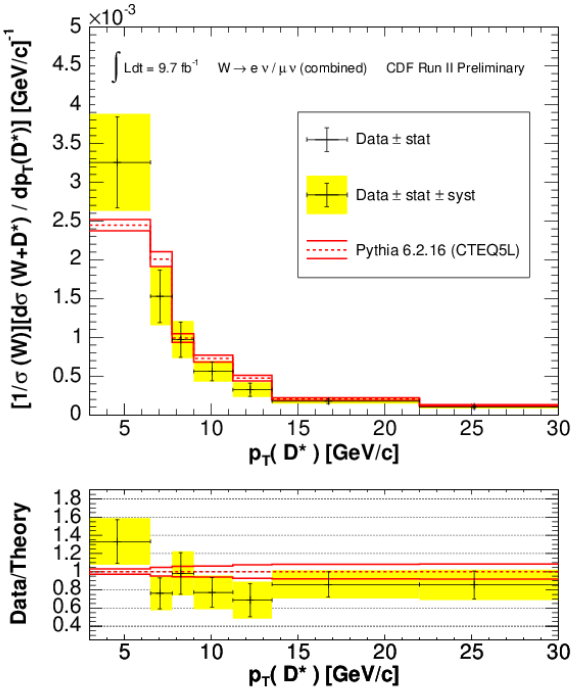

FIG. 6: The ratio of physical cross-sections $\sigma(W + D^*)/\sigma(W)$ as a function of $p_T(D^*)$, for combined $W \to e\nu$ and $W \to \mu\nu$ results. Combination is made using a best linear uncertainty estimate with systematic uncertainties assumed to be fully correlated. The displayed restrictions on $p_T(D^*)$ are the only kinematic restriction on these results. In each case, error bars give the statistical uncertainty, while the sum in quadrature of the statistical and systematic errors is shown as a yellow error band. The dotted red line shows the prediction of the Pythia 6.2 obtained using the CTEQ5L PDF set, with solid red lines showing PDF uncertainty in this prediction. The ratio of the simulated distribution to data is shown in the lower panels.

Production process	Fraction of $W(\to \ell\nu) + D^*$ signal
$s(d) + g \to W + c$	$14 \pm 6\%$
$q + \bar{q}' \to W + g(\to c\bar{c})$	$73 \pm 8\%$
$q + \bar{q}' \to W + g(\to b\bar{b})$	$13 \pm 5\%$

TABLE VI: The fraction of our tagged $W + D^*$ signal that comes from each of the three production processes that are expected to contribute. The $q + \bar{q}' \to W + g(\to b\bar{b})$ fraction comes from our NN-based approach (Section V A), while our $q + g \to W + c$ fraction comes from the D^* and W sign correlation-based approach (Section V B).

IX. SUMMARY

By fully-reconstructing $D^*(2010) \to D^0(\to K\pi)\pi_s$ decays in W/Z events, we measure the rate of D^* production in association with W and Z bosons. Full reconstruction allows us to describe $W/Z + D^*$ production in a lower-p_T region than had previously been explored. We present a first measurement of $W/Z + D^*$ rates at the Tevatron in the regime $p_T(D^*) > 3$ GeV. We find that the expected rate of D^* production is as predicted by Pythia 6.2, both for the integrated sample $p_T(D^*) > 3$ GeV, and differentially as a function of $p_T(D^*)$.

This analysis should be viewed as a complement to higher-p_T charm analyses which identify charm via jet tagging. By exploring the lower-p_T charm regime, this analysis helps to generate a fuller picture for understanding heavy flavor production in association with vector boson events.

Acknowledgments

We thank the Fermilab staff and the technical staffs of the participating institutions for their vital contributions. This work was supported by the U.S. Department of Energy and National Science Foundation; the Italian Istituto Nazionale di Fisica Nucleare; the Ministry of Education, Culture, Sports, Science and Technology of Japan; the Natural Sciences and Engineering Research Council of Canada; the National Science Council of the Republic of China; the Swiss National Science Foundation; the A.P. Sloan Foundation; the Bundesministerium fuer Bildung und Forschung, Germany; the Korean Science and Engineering Foundation and the Korean Research Foundation; the Particle Physics and Astronomy Research Council and the Royal Society, UK; the Russian Foundation for Basic Research; the Comision Interministerial de Ciencia y Tecnologia, Spain; and in part by the European Community's Human Potential Programme under contract HPRN-CT-20002, Probe for New Physics.

[1] The CDF II Collaboration, *CDF II Detector Technical Design Report*, Tech. Rep. FERMILAB-Pub-96/390-E (1996).
[2] H. L. et. al., JHEP **0704** (2007).
[3] U. B. et. al., Phys. Lett. **B318** (1993).
[4] T. A. et. al., "CDF Public Note 10704," (2012).
[5] *Charm Physics at CDF*, FERMILAB-CONF-12-210-E (2012).
[6] E. L. S. Keller, W.T. Giele, Phys. Lett. **B372** (1996).
[7] T. A. et. al., Phys. Rev. Lett. **100** (2008).
[8] T. A. et. al., Phys. Rev. Lett. **110** (2013).
[9] V. A. et. al., Phys. Rev. Lett. **112** (2014).
[10] J. B. et. al. (Particle Data Group), Phys. Rev. D **86** (2012).